1

Introduction

1.1 The atmospheric radiation field

The theory presented in this book applies to the lower 50 km of the Earth's atmosphere, that is to the troposphere and to the stratosphere. In this part of the atmosphere the so-called *local thermodynamic equilibrium* is observed.

In general, the condition of *thermodynamic equilibrium* is described by the state of matter and radiation inside a constant temperature enclosure. The radiation inside the enclosure is known as *black body radiation*. The conditions describing thermodynamic equilibrium were first formulated by Kirchhoff (1882). He stated that within the enclosure the radiation field is:

(1) isotropic and unpolarized;
(2) independent of the nature and shape of the cavity walls;
(3) dependent only on the temperature.

The existence of local thermodynamic equilibrium in the atmosphere implies that a local temperature can be assigned everywhere. In this case the *thermal radiation* emitted by each atmospheric layer can be described by *Planck's radiation law*. This results in a relatively simple treatment of the thermal radiation transport in the lower sections of the atmosphere.

Kirchhoff's and Planck's laws, fundamental in radiative transfer theory, will be described in the following chapters. While the derivation of Planck's law requires a detailed microscopic picture, Kirchhoff's law may be obtained by using purely thermodynamic arguments. The derivation of Kirchhoff's law is presented in numerous textbooks such as in *Thermodynamics of the Atmosphere* by Zdunkowski and Bott (2004).[1]

[1] Whenever we make reference to this book, henceforth we simply refer to THD (2004).

The atmosphere, some sort of an open system, is not in thermodynamic equilibrium since the temperature and the radiation field vary in space and in time. Nevertheless, in the troposphere and within the stratosphere the *emission* of thermal radiation is still governed by Kirchhoff's law at the local temperature. The reason for this is that in these atmospheric regions the density of the air is sufficiently high so that the mean time between molecular collisions is much smaller than the mean lifetime of an excited state of a radiating molecule. Hence, equilibrium conditions exist between *vibrational* and *rotational* and the *translational energy* of the molecule. At levels higher than 50 km, the two time scales become comparable resulting in a sufficiently strong deviation from thermodynamic equilibrium so that Kirchhoff's law cannot be applied anymore.

The breakdown of thermodynamic equilibrium in higher regions of the atmosphere also implies that Planck's law no longer adequately describes the *thermal emission* so that quantum theoretical arguments must be introduced to describe radiative transfer. Quantum theoretical considerations of this type will not be treated in this book. For a study of this situation we refer the reader to the textbook *Atmospheric Radiation* by Goody and Yung (1989).

The units usually employed to measure the wavelength of radiation are the micrometer (μm) with $1\,\mu\text{m} = 10^{-6}$ m or the nanometer (nm) with $1\,\text{nm} = 10^{-9}$ m and occasionally Ångströms (Å) where $1\,\text{Å} = 10^{-10}$ m. The thermal radiation spectrum of the Sun, also called the *solar radiation spectrum*, stretches from roughly 0.2–3.5 μm where practically all the thermal energy of the solar radiation is located. It consists of ultraviolet radiation ($< 0.4\,\mu\text{m}$), visible radiation (0.4–0.76 μm), and infrared radiation $> 0.76\,\mu\text{m}$. The thermal radiation spectrum of the Earth ranges from about 3.5–100 μm so that for all practical purposes the solar and the terrestrial radiation spectrum are separated. As will be seen later, this feature is of great importance facilitating the calculation of atmospheric radiative transfer. Due to the positions of the spectral regions of the solar and the terrestrial radiation we speak of *short-wave* and *long-wave radiation*. The terrestrial radiation spectrum is also called the *infrared radiation spectrum*.

Important applications of atmospheric radiative transfer are climate modeling and weather prediction which require the evaluation of a prognostic temperature equation. One important term in this equation, see e.g. Chapter 3 of THD (2004), is the divergence of the *net radiative flux density* whose evaluation is fairly involved, even for conditions of local thermodynamic equilibrium. Accurate numerical radiative transfer algorithms exist that can be used to evaluate the radiation part of the temperature prediction equation. In order to judiciously apply any such computer model, some detailed knowledge of radiative transfer is required.

There are other areas of application of radiative transfer such as remote sensing. In the concluding chapter of this textbook we will present various examples.

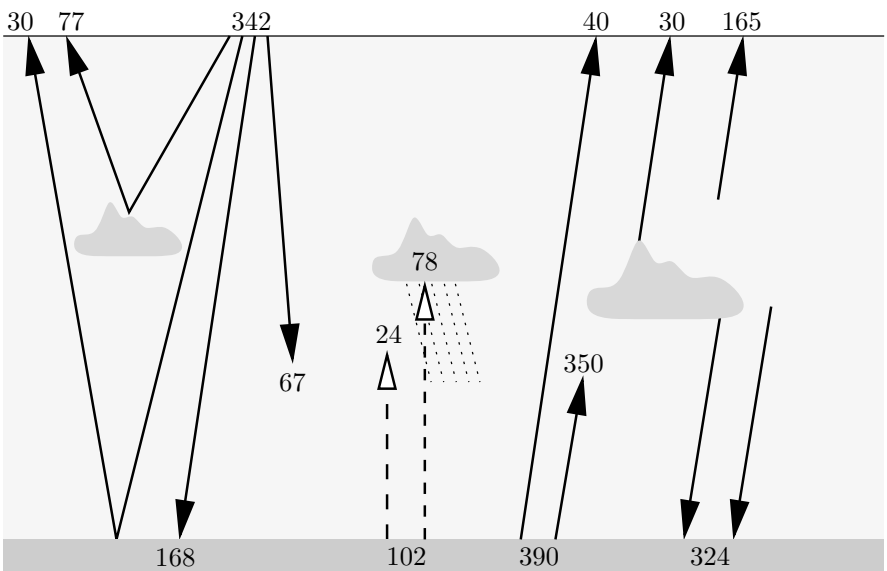

Fig. 1.1 The Earth's annual global mean energy budget, after Kiehl and Trenberth (1997), see also Houghton *et al.* (1996). Units are (W m^{-2}).

1.2 The mean global radiation budget of the Earth

Owing to the advanced satellite observational techniques now at our disposal, we are able to study with some confidence the Earth's annual mean global energy budget. Early meteorologists and climatologists have already understood the importance of this topic, but they did not have the observational basis to verify their results. A summary of pre-satellite investigations is given by Hunt *et al.* (1986). In the following we wish to briefly summarize the mean global radiation budget of the Earth according to Kiehl and Trenberth (1997). Here we have an instructive example showing in which way radiative transfer models can be applied to interpret observations.

The evaluation of the radiation model requires vertical distributions of absorbing gases, clouds, temperature, and pressure. For the major absorbing gases, namely water vapor and ozone, numerous observational data must be handled and supplemented with model atmospheres. In order to calculate the important influence of CO_2 on the infrared radiation budget, Kiehl and Trenberth specify a constant volume mixing ratio of about 350 ppmv. Moreover, it is necessary to employ distributions of the less important absorbing gases CH_4, N_2O, and of other trace gases. Using the best data presently available, they have provided the radiation budget as displayed in Figure 1.1.

The analysis employs a *solar constant* $S_0 = 1368\,\mathrm{W\,m^{-2}}$. This is the solar radiation, integrated over the entire solar spectral region which is received by the Earth per unit surface perpendicular to the solar beam at the mean distance between the Earth and the Sun. Since the circular cross-section of the Earth is exposed to the parallel solar rays, each second our planet receives the energy amount $\pi R^2 S_0$ where R is the radius of the Earth. On the other hand, the Earth emits infrared radiation from its entire surface $4\pi R^2$ which is four times as large as the cross-section. Thus for energy budget considerations we must distribute the intercepted solar energy over the entire surface so that, on the average, the Earth's surface receives 1/4 of the solar constant. This amounts to a solar input of $342\,\mathrm{W\,m^{-2}}$ as shown in the figure.

The measured solar radiation reflected to space from the Earth's surface–atmosphere system amounts to about $107\,\mathrm{W\,m^{-2}}$. The ratio of the reflected to the incoming solar radiation is known as the *global albedo* which is close to 31%. Early pre-satellite estimates of the global albedo resulted in values ranging from 40–50%. With the help of radiation models and measurements it is found that cloud reflection and scattering by atmospheric molecules and aerosol particles contribute $77\,\mathrm{W\,m^{-2}}$ while ground reflection contributes $30\,\mathrm{W\,m^{-2}}$. In order to have a balanced radiation budget at the top of the atmosphere, the net gain $342 - 107 = 235\,\mathrm{W\,m^{-2}}$ of the short-wave solar radiation must be balanced by emission of long-wave radiation to space. Indeed, this is verified by satellite measurements of the outgoing long-wave radiation.

Let us now briefly consider the radiation budget at the surface of the Earth, which can be determined only with the help of radiation models since sufficiently dense surface measurements are not available. Assuming that the ground emits black body radiation at the temperature of 15°C, an amount of $390\,\mathrm{W\,m^{-2}}$ is lost by the ground. According to Figure 1.1 this energy loss is partly compensated by a short-wave gain of $168\,\mathrm{W\,m^{-2}}$ and by a long-wave gain of $324\,\mathrm{W\,m^{-2}}$ because of the thermal emission of the atmospheric *greenhouse gases* (H_2O, CO_2, O_3, CH_4, etc.) and clouds. Thus the total energy gain $168 + 324 = 492\,\mathrm{W\,m^{-2}}$ exceeds the long-wave loss of $390\,\mathrm{W\,m^{-2}}$ by $102\,\mathrm{W\,m^{-2}}$.

In order to have a balanced energy budget at the Earth's surface, other physical processes must be active since a continuous energy gain would result in an ever increasing temperature of the Earth's surface. From observations, Kiehl and Trenberth estimated a mean global precipitation rate of $2.69\,\mathrm{mm\,day^{-1}}$ enabling them to compute a surface energy loss due to evapotranspiration. Multiplying $2.69\,\mathrm{mm\,day^{-1}}$ by the density of water and by the latent heat of vaporization amounts to a latent heat flux density of $78\,\mathrm{W\,m^{-2}}$. Thus the surface budget is still unbalanced by $24\,\mathrm{W\,m^{-2}}$. Assigning a surface energy loss of $-24\,\mathrm{W\,m^{-2}}$ resulting from sensible heat fluxes yields a balanced energy budget at the Earth's surface. The individual

losses due to turbulent surface fluxes are uncertain within several percent since it is very difficult to accurately assess the global amount of precipitation which implies that the estimated sensible heat flux density is also quite uncertain. Only the sum of the turbulent surface flux densities is reasonably certain.

Finally, we must study the budget of the atmosphere itself. Figure 1.1 reveals that the atmosphere gains 67 W m^{-2} by absorption of solar radiation, 102 W m^{-2} by turbulent surface fluxes, and additionally 350 W m^{-2} resulting from long-wave radiation emitted by the surface of the Earth and intercepted by atmospheric greenhouse gases and clouds. The total of 519 W m^{-2} must be re-emitted by the atmosphere. As shown in the figure, the atmospheric greenhouse gases and the clouds emit $165 + 30 = 195$ W m^{-2} to space and 324 W m^{-2} as back-radiation to the surface of the Earth just balancing the atmospheric energy gain.

We also see that from the 390 W m^{-2} emitted by the Earth's surface only 350 W m^{-2} are intercepted by the atmosphere. To account for the remaining 40 W m^{-2} we recognize that these escape more or less unimpeded to space in the so-called *spectral window region* as will be discussed later.

By considering the budget in Figure 1.1, we observe that only the reflected solar radiation and the long-wave radiation emitted to space are actually verified by measurements. However, the remaining budget components should also be taken seriously since nowadays radiation models are quite accurate. Nevertheless, the output of the models cannot be any more accurate than the input data. In future days further refinements and improvements of the global energy budget can be expected.

In order to calculate the global radiation budget, we must have some detailed information on the absorption behavior of atmospheric trace gases and the physical properties of aerosol and cloud particles. In a later chapter we will study the radiative characteristics of spherical particles by means of the solution of *Maxwell's equations* of electromagnetic theory. Here we will only qualitatively present the absorption spectrum of the most important greenhouse gases.

Figure 1.2 combines some important information regarding the solar spectrum. The upper curve labeled TOA (top of the atmosphere) shows the extraterrestrial incoming solar radiation after Coulson (1975). For wavelengths exceeding 1.4 μm this curve coincides closely with a Planckian black body curve of 6000 K. The lower curve depicts the total solar radiation reaching the Earth's surface for a solar zenith angle $\theta_0 = 60^\circ$. The calculations were carried out with sufficiently high spectral resolution using the so-called Moderate Resolution Atmospheric Radiance and Transmittance Model (MODTRAN; version 3.5; Anderson, 1996; Kneizys *et al.*, 1996) program package. All relevant absorbing trace gases shown in the figure are included in the calculations. Not shown are the positions of the CO and CH_4 absorption bands which are located in the solar spectrum and in the near infared spectral region of

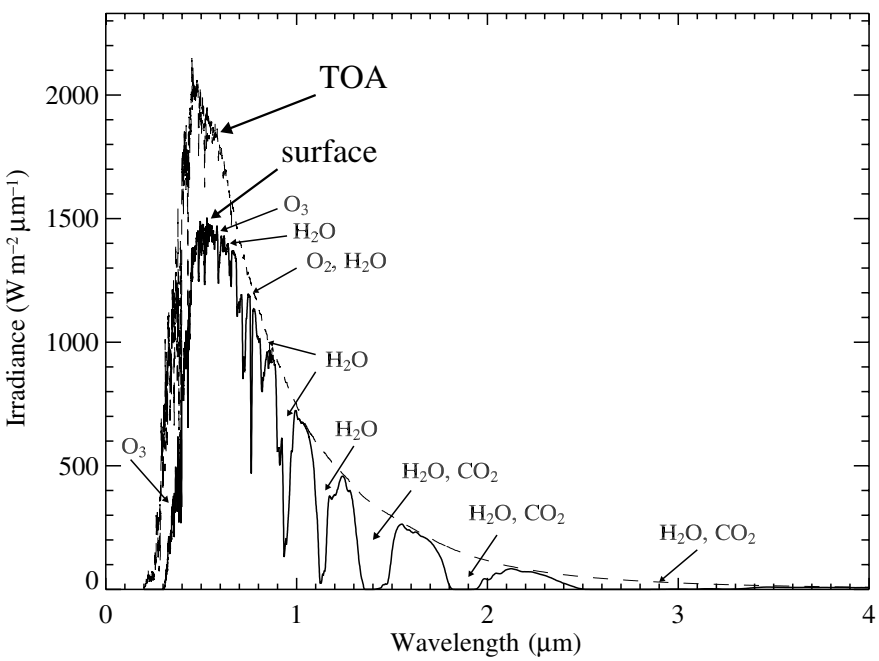

Fig. 1.2 Incoming solar flux density at the top of the atmosphere (TOA) and at ground level. The solar zenith angle is $\theta_0 = 60^\circ$, ground albedo $A_g = 0$. The spectral positions of major absorption bands of the trace gases are shown.

thermal radiation. A tabulation of bands of these two trace gases is given, for example, in Goody (1964a). Since the radiation curve for ground level shows a high spectral variability, it was artificially smoothed for better display to a somewhat lower spectral resolution.

Figure 1.3 depicts the spectral distribution of the upwelling thermal radiance as a function of the wave number (to be defined later) at a height of 60 km. For comparison purposes the Planck black body radiance curves for several temperatures are shown also. The maximum of the 300 K black body curve is located at roughly 600 cm^{-1}. The calculations were carried out with the same program package (MODTRAN) using a spectral resolution of 1 cm^{-1}. All relevant absorbing and emitting gases have been accounted for. The widths of the major infrared absorption bands (H_2O, CO_2, O_3) are also shown in the figure.

Kiehl and Trenberth (1997) produced similar curves for the solar and infrared radiative fluxes per unit surface. However, in addition to the absorption by gases shown in Figures 1.2 and 1.3, they also included the effects of clouds in their calculations by assuming an effective droplet radius of 10 µm and suitable liquid water contents. Moreover, assumptions were made about the spatial distributions of clouds. Their results indicate that water vapor is the most important

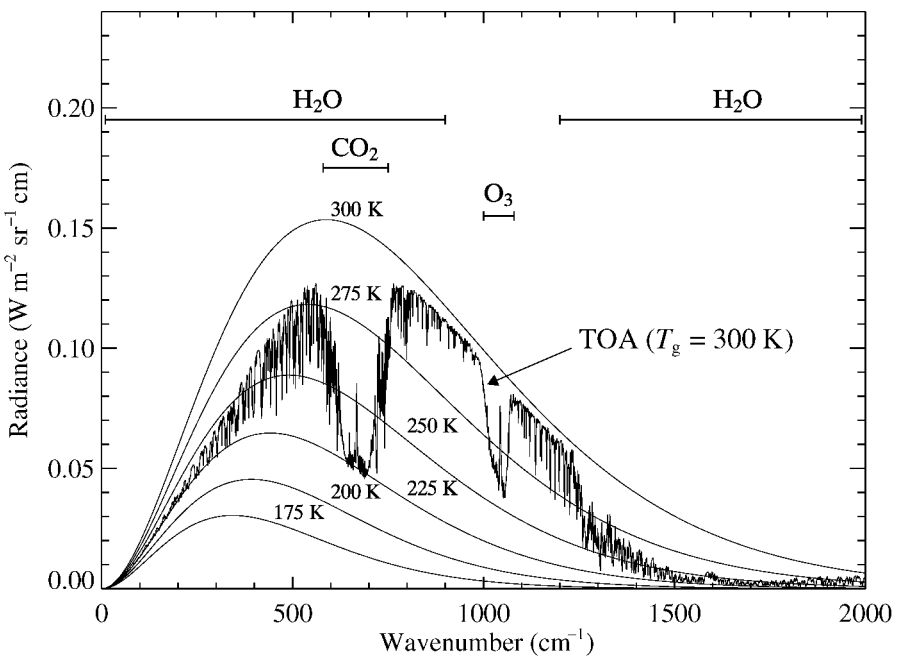

Fig. 1.3 Upwelling infrared radiance at a height of 60 km for a clear sky mid-latitude summer atmosphere.

gas absorbing 38 W m^{-2} of solar radiation which is followed by O_3 (15 W m^{-2}) and O_2 (2 W m^{-2}) while the effect of CO_2 may be ignored. Thus the greenhouse gases absorb 55 W m^{-2}. Figure 1.1, however, requires 67 W m^{-2}. The 12 W m^{-2} still missing must be attributed to partial cloudiness and to spectral overlap effects, i.e., cloud droplets and gases absorb at the same wavelength. Handling clouds in the radiative transfer problem is usually very difficult since in general water droplet size distributions are unknown.

Finally, let us consider the gaseous absorption bands of the infrared spectrum. In the calculations of Kiehl and Trenberth (1997) analogous to Figure 1.3, the surface is assumed to emit black body radiation with a temperature of 15°C. The major absorbing gases are H_2O, O_3, and CO_2. Of course, the same distribution of absorbing gases and clouds as for solar radiation is assumed. Integration of the infrared curve at the top of the atmosphere over the entire spectral region yields 235 W m^{-2} as required by Figure 1.1.

We conclude this section by considering a simple example to obtain the effective emission temperature of the system Earth's surface–atmosphere. As we have discussed above, the cross-section of the Earth intercepts the solar energy $\pi R^2 S_0$. Since the global albedo is 31%, the rate of absorption is $1368(1-0.31) = 944$ W m^{-2}. Assuming that the Earth emits black body radiation, we must apply the

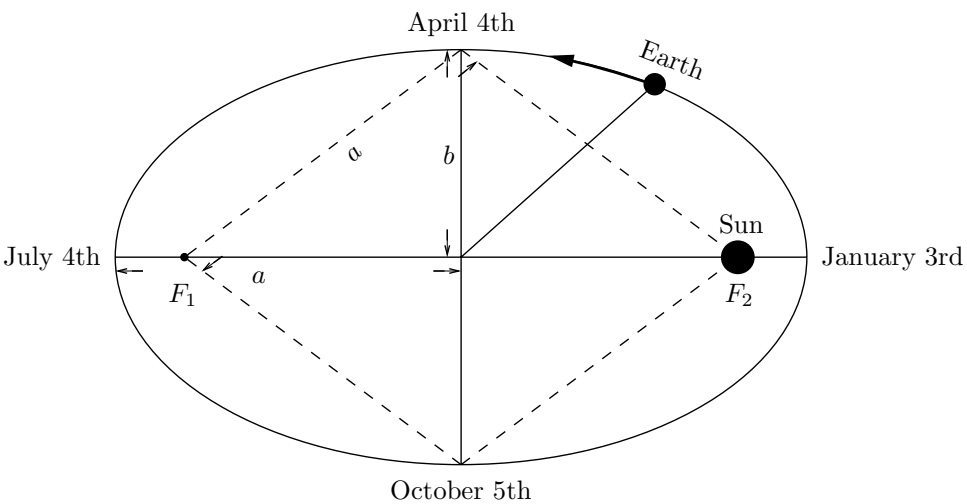

Fig. 1.4 Simplified elliptical geometry of the Earth's orbit.

well-known *Stefan–Boltzmann law* so that the Earth's surface emits $4\pi R^2\sigma T^4$ where σ is the *Stefan–Boltzmann constant*. Assuming steady-state conditions, we have $\pi R^2 \times 944\ \mathrm{W\ m^{-2}} = 4\pi R^2\sigma T^4$ from which we obtain the temperature $T = 254$ K which resembles the effective emission temperature of our planet.

1.3 Solar–terrestrial relations

To a high degree of accuracy the Earth's orbit around the Sun can be described by an ellipse with eccentricity $e = \sqrt{a^2 - b^2}/a = 0.01673$, where a and b are, respectively, the semi-major and semi-minor axis of the ellipse, see Figure 1.4. The Sun's position is located in one of the two elliptical foci (F_1, F_2). For demonstration purposes, the figure exaggerates the eccentricity of the elliptical orbit. The *perihelion*, that is the shortest distance $r_{\min}$ between Sun and Earth, occurs around January 3rd, while the *aphelion*, that is the largest distance $r_{\max}$ between Sun and Earth, is registered around July 4th. These times are not constant, but they vary from year to year. Often the mean distance between the Earth and the Sun is approximated by

$$a = \frac{r_{\min} + r_{\max}}{2} = 1.496 \times 10^8\,\mathrm{km} \tag{1.1}$$

The distances $r_{\min}$ and $r_{\max}$ are related to a and e via

$$\begin{aligned} r_{\min} &= a(1-e) = 1.471 \times 10^8\,\mathrm{km} \\ r_{\max} &= a(1+e) = 1.521 \times 10^8\,\mathrm{km} \end{aligned} \tag{1.2}$$

Beginning with January 1st, i.e. Julian day number 1 of the year, a normal year counts 365 days (for simplicity we will not take the occurrence of leap years into account). A particular day of the year is then labelled with its corresponding Julian day number J.

We introduce the rotation angle Γ of the Earth beginning with the 1st of January as

$$\Gamma = \frac{2\pi}{365}(J-1) \tag{1.3}$$

where Γ is expressed in radians.

During the course of the year the angular distance Sun–Earth, the *solar declination* δ, and the so-called *equation of time* ET change in a more or less harmonic manner. In the following we will discuss simple expressions developed by Spencer (1971) which are accurate enough to evaluate the quantities $(a/r)^2$, δ, and ET, where r is the actual distance between Sun and Earth. The term $(a/r)^2$ is given by

$$\left(\frac{a}{r}\right)^2 = 1.000110 + 0.034221\cos\Gamma + 0.001280\sin\Gamma + 0.000719\cos 2\Gamma + 0.000077\sin 2\Gamma \tag{1.4}$$

with a maximum error of approximately 10^{-4}. If $S_0 = 1368\,\mathrm{W\,m^{-2}}$ is the *solar constant* for the mean distance between Sun and Earth, the actual solar constant varies as a function of J

$$S_0(J) = S_0\left(\frac{a}{r(J)}\right)^2 \tag{1.5}$$

According to (1.4) the maximum change of $S_0(J)$ relative to S_0 has an amplitude of approximately 3.3%.

The solar declination δ is defined as the angle between the Earth's equatorial plane and the actual position of the Sun as seen from the center of the Earth. The Earth's rotational axis and the normal to the Earth's plane of the ecliptic make on average an angle of $\varepsilon = 23^\circ 27'$, δ amounts to $+23^\circ 27'$ and $-23^\circ 27'$ at summer solstice (around June 21st) and winter solstice (around December 22nd), respectively. These relations are illustrated in Figure 1.5 and in the three-dimensional view of the Sun–Earth geometry of Figure 1.6.

The *equinox points* are defined as the intersecting line (equinox line) between the Earth's plane of the ecliptic and the Sun's equatorial plane. A second line which is normal to the equinox line and which is located in the Earth's plane of the ecliptic intersects the Earth's orbit in the points WS (winter solstice) and SS (summer solstice). The perihelion P and the aphelion A, which both lie on the semi-major axis of the Earth's elliptical orbit, make an angle $\psi = 11^\circ 08'$ with the solstice line.

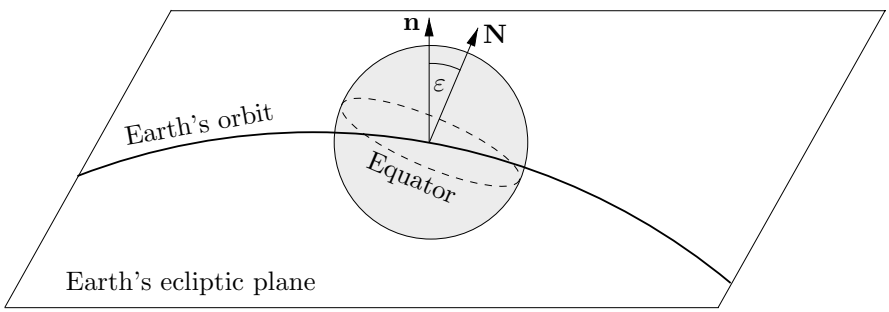

Fig. 1.5 Relation between the Earth's orbit, the normal vector **n** to the plane of the ecliptic, the Earth's rotational vector **N** and the angle of the ecliptic ε.

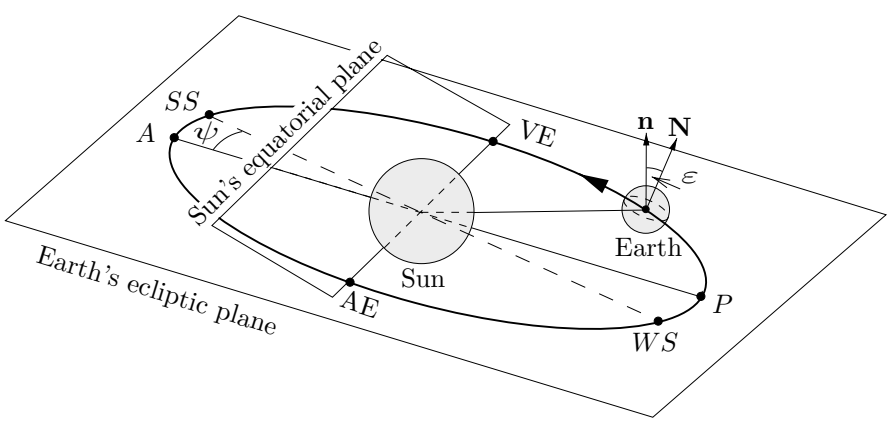

Fig. 1.6 Schematical view of the Sun–Earth geometry. P, perihelion; VE, vernal equinox; SS, summer solstice; A, aphelion; AE, autumnal equinox; WS, winter solstice; ε, angle of the ecliptic; ψ, angle between the distances (SS, WS) and (A, P); **N**, vector along the rotational axis of the Earth; **n**, normal unit vector with respect to the Earth's plane of the ecliptic.

It should be observed that the vector **N** is fixed in direction pointing to the polar star. At the solstices the vectors **N**, **n** and the line between the solstice points lie in the same plane so that $\delta = \pm 23^{\circ}27'$. At the equinox points ($\delta = 0^{\circ}$) the line between the Earth and the Sun is at a right angle to the line (SS, WS).

The solar declination δ is a function of the Julian day number J. It can be expressed as

$$\begin{aligned}\delta = {} & 0.006918 - 0.399912\cos\Gamma + 0.070257\sin\Gamma \\ & - 0.006758\cos 2\Gamma + 0.000907\sin 2\Gamma \end{aligned} \tag{1.6}$$

with δ expressed in radians. Due to Spencer (1971) this approximate formula has an error in δ less than $12'$. Figure 1.7 depicts a plot of δ versus J.